

Rochester Institute of Technology

## RIT Digital Institutional Repository

---

Presentations and other scholarship

Faculty & Staff Scholarship

---

8-8-1993

### A 193 nm Deep-UV Lithography System Using a Line-Narrowed ArF Excimer Laser

Bruce W. Smith

*Rochester Institute of Technology*

Malcolm Gower

*Exitech Ltd.*

Mark Westcott

*GCA Tropel*

Lynn F. Fuller

*Rochester Institute of Technology*

Follow this and additional works at: <https://repository.rit.edu/other>

---

#### Recommended Citation

Bruce W. Smith, Malcolm C. Gower, Mark Westcott, Lynn F. Fuller, "193-nm deep-UV lithography system using a line-narrowed ArF excimer laser", Proc. SPIE 1927, Optical/Laser Microlithography, (8 August 1993); doi: 10.1117/12.150488; <https://doi.org/10.1117/12.150488>

This Conference Paper is brought to you for free and open access by the RIT Libraries. For more information, please contact [repository@rit.edu](mailto:repository@rit.edu).

# A 193 nm deep-UV lithography system using a line-narrowed ArF excimer laser

Bruce W. Smith<sup>†</sup>, Malcolm C. Gower<sup>‡</sup>, Mark Westcott<sup>§</sup>, Lynn F. Fuller<sup>†</sup>

<sup>†</sup>Rochester Institute of Technology  
Microelectronic Engineering Department  
Rochester, New York 14623

<sup>‡</sup>Exitech Limited, Hanborough Park, Long Hanborough, Oxford OX8 8LH

<sup>§</sup>GCA Tropel, Fairport, New York, 14450

## ABSTRACT

A small field refractive projection system for operation at the 193.3 nm wavelength of a spectrally narrowed ArF excimer laser is being constructed. The 1 mm field, 20X system operates with a variable objective lens numerical aperture from 0.30 to 0.60, variable partial coherence, and control over illumination fill and mask tilt. A 30 W maximum power ArF excimer laser has been spectrally line-narrowed through incorporation of tilted Fabry-Perot etalons into the laser cavity, allowing linewidths on the order of  $7 \text{ cm}^{-1}$  (26 pm) with one etalon and  $0.5 \text{ cm}^{-1}$  (2pm) with two etalons. This work reports laser line narrowing and lens performance results. Simulations of aerial image intensity distributions from lens aberration data will be presented for 0.25 and 0.20 micron geometry.

## 1. INTRODUCTION

Excimer laser projection lithography using the 248 nm, KrF excimer laser has been demonstrated for sub-half micron lithography. Through various image modification schemes, including phase masking, illumination alteration, and spatial filtering, 0.25 micron imaging may be possible using tools operating at this wavelength. In order to approach sub-quarter micron resolution with optical tools, shorter exposure wavelengths may need to be utilized. Several efforts are under way to utilize the 193.3 wavelength of the ArF excimer laser<sup>1,2,3,4</sup>. Imaging at wavelengths below 200 nm presents many problems, with increasingly fewer materials transparent to exposing radiation. Consequently, most programs have been directed toward partial or complete reflection systems, eliminating the difficulties involved with the line narrowing an ArF excimer laser and placing little demand on the spectral bandwidth of the source. This work involves the development of 193 nm imaging capabilities for sub-quarter micron resolution using all-refractive optical components. We have addressed the feasibility of such an approach by constructing a small-field process development system for imaging studies and material evaluation based on the GCA-BOLD (Basic Optical Lithography Device) using an excimer laser spectrally narrowed with intra-cavity etalons.<sup>5</sup>

## 2. ArF EXCIMER SOURCE

The availability and performance of optical materials at 193 nm limits choices for refractive lens design and manufacture. Of the few transmissive materials available, only fused silica is a practical choice for lens fabrication because of its mechanical, thermal and chemical stability. This lack of suitable optical materials at 193.3 nm forces spectral constraints upon the laser source, requiring operation at or near 2  $\mu\text{m}$  for reduction of chromatic aberration in large field lenses. Several techniques have been utilized for spectral bandwidth narrowing of excimer lasers, including the use of diffraction gratings, prisms, and etalons. An etalon approach has been employed because of its high efficiency and versatility as an external optical component to an excimer laser. The use of intracavity fixed air gap Fabry-Perot etalons in the unrestricted aperture the excimer laser head allows for maximum output at narrow spectral bandwidths and has been utilized for lasers operating 308 nm (XeCl) and 248 nm (KrF) with narrowing efficiencies of 25%.<sup>6,7</sup> A single tilted Fabry-Perot etalon in a KrF excimer cavity has been used to produce a bandwidth on the order of 25 nm. Tuning is achieved by adjusting tilt angle, which is varied in the plane of the smaller beam dimension. Insertion of a second tilted etalon with a free spectral range approximately equal to the linewidth produced by one etalon can narrow further to the 2 to 3 nm range.

For use in an ArF excimer laser, the dual Fabry-Perot etalon approach becomes more challenging. The reduced gain for operation with ArF combines with the losses due to lower transmissions of laser optics, decreasing narrowing efficiencies. Pulse durations of 10-20 nsec result in laser emission from very few round trip laser passes. Additional energy loss processes occurring during laser operation require operation with cryogenic gas purification. Expected efficiencies for a highly-narrowed ArF laser are, therefore, lower than those for higher operating wavelength rare gas halogens, from 25% efficient to near 15%. The incorporation of the tilted dual-etalons into the laser cavity is shown in Figure 1. Lumonics EX-700 and a Questek 2840 excimer lasers have been operated using ArF with this configuration. To measure the spectral output from the laser, a high resolution laser spectrometer incorporating an echelle Littrow grating was used. Output for broadband, single (coarse) etalon, and dual (fine) operation are shown in Figure 2. Approximate output energy for operation in the broadband mode for the Lumonics EX700 is 300 mJ/pulse. The Questek 2840 operates near 400 mJ/pulse broadband. Operation with a single etalon will decrease energy to approximately 50%, while operation with dual etalons decreases to approximately 15%. Manual wavelength tuning is currently possible during ArF operation. Wavelength stabilized operation can be made possible though locking the laser output to a calibrated laser line, such as that of a HeNe laser.

## 3. OPTICAL SYSTEM

The projection optical system is based on the GCA BOLD 20X imaging system. The objective is a variable numerical aperture (0.3 to 0.6) all refractive, six element lens with a 1mm approximate field diameter. The object to image distance is 315.43 mm, the effective focal length is 12.85 mm, and the entrance pupil is located 257.04 mm from the object. Focus is manually selected by control of the mask position at 20X. The small number of optical elements in the projection lens reduces transmission loss, which would be encountered in the typical lens design

consisting of 20 to 30 elements. Additionally, the short focal length and 20X magnification relaxes the requirement of source bandwidth to 7 pm for 0.60 NA, as calculated from the first order approximation to source bandwidth for one half Rayleigh focal depth:

$$\Delta\lambda(FWHM) = \frac{(n-1)\lambda}{2f(1+m)\left(\frac{\partial n}{\partial \lambda}\right)NA^2}$$

Here,  $n$  is refractive index of the lens material,  $f$  is focal length,  $m$  is magnification (0.05), and  $\frac{\partial n}{\partial \lambda}$  is the dispersion of the lens material. Furthermore, a FWHM bandwidth of 26 pm is the minimum requirement for 0.30 NA, which can be obtained with a single etalon in the excimer laser cavity. A single blank of UV grade fused silica with OH concentration in the range of 1000 ppm was used for lens manufacture. Transmission loss of 31% is estimated through the total 40.6 mm lens glass thickness as a result of bulk absorbance and scattering. The illuminator incorporates a variable entrance aperture, allowing control of partial coherence,  $\sigma$ , from near 0 to near 1.0. This allows optimization of NA and  $\sigma$  for feature size, type, and parity. Access to the aperture also allows for alternative illumination schemes, such as off-axis illumination. The system configuration is shown in Figure 3.

#### 4. IMAGING CAPABILITIES

Because the projection lens has a field size of 1 mm, lens complexity is reduced and aberration-free images can be obtained within a numerical aperture range of 0.30 to 0.60. Wavefront data from lens design, represented by Fringe Zernike polynomial coefficient terms, are shown in Table 1 for axis, 0.70, and edge field positions at 193.3 nm and at a +2 pm deviation from the exposing wavelength (NA=0.60). Index values for fused silica were extrapolated using a Malitson technique<sup>8,9</sup>, and were considered accurate to +/- 0.0001. Waveform deformation (OPD) plots for -0.3 to 0.3 microns of defocus at 0.70 and full field positions are shown in Figure 4. Total wavefront distortion remains below one fifth wave to full field. Interferometric measurements of the lens have not been performed at 193.3 nm, but at 248.4 nm on-axis. Minimization of aberrations over the entire field will be accomplished through experimental optimization techniques.

The performance capabilities of the projection system have been investigated through simulations using DEPICT-2, a projection lens model capable of simulating the effects of high-order lens aberration<sup>10</sup>. Through specification of Zernike lens aberration coefficients, two-dimensional aerial image intensity distributions were calculated and plotted for 0.25 micron and 0.20 micron features on 0.70 and full field position for 0.60 NA and  $\sigma = 0.50$  (Figure 5). Constant value contours correspond to 12.5% for all cases. Rotations within the field position of 0, 45, and 90 degrees are compared to an ideal aberration free aerial image. Y tilt can be detected at full field, 90 degrees but can be corrected for. 3rd and 5th order Y coma (terms 8 and 15) account considerably for error at 0.70 and full field. One dimensional aerial image intensity plots are shown in Figure 6, for 0.25 micron and 0.20 micron features at 0.60 NA for +0.45 microns of defocus. Aerial image modulation,  $(I_{max} - I_{min}) / (I_{max} + I_{min})$ , is calculated for each case. Image modulation above 95% can be obtained for 0.25 micron features at full field and modulation above 91% can be obtained for 0.20 micron features, if best focus is maintained.

Pattern transfer with these levels of modulation presents no difficulty in single level resist materials. A 50% image modulation is maintained for 0.20 micron lines within a focal range of +/- 0.35 micron, also within the capabilities of single layer materials such as PMMA. Top-surface imaging techniques may extend capabilities to allow image modulation to 20%, allowing 0.20 micron features defocused to +/- 0.6 micron or 0.15 micron features in a focal range of +/- 0.3 micron.

## 5. CONCLUSIONS

An 193 nm refractive lithography system for research applications has been constructed based on the GCA BOLD and an ArF excimer laser narrowed with tilted Fabry-Perot etalons. With the ability to control imaging parameters, such as lens NA and  $\sigma$ , illumination, mask tilt, wavelength shift, and mask type, imaging studies and resist characterization at 193 nm are possible. Features to 0.20 micron are possible and features to 0.15 micron may be achievable with high contrast resist processes, such as top-surface imaging.

## REFERENCES

- <sup>1</sup> D.C. Shaver, D.M. Craig, C.A. Marchi, M.A. Hartney, SPIE, vol. 1674, pp. 766-775 (1992).
- <sup>2</sup> G. Owen, R.F.W. Pease, D.A. Markle, J. Vac. Sci. Technol. B 10(6), pp. 3032-3036 (1992).
- <sup>3</sup> M. Rothschild, R.B. Goodman, M.A. Hartney, M.W. Horn, R.R. Kunz, J.H.C. Sedlacek, D.C. Shaver, J. Vac. Sci Technol. B 10(6), pp. 2989-2996 (1992).
- <sup>4</sup> M. Sasago, Y. Tani, M. Endo, N. Nomura, SPIE vol. 1264, pp. 466-476 (1990).
- <sup>5</sup> J. H. Bruning, W. Oldham, SPIE vol. 922, pp. 471-475 (1988).
- <sup>6</sup> P. T. Rumsby and M.C. Gower, IEEE LEOS, UV3.3, (1988).
- <sup>7</sup> M.C. Gower, C. Willimas, P. Apte, P.T. Rumsby, SPIE OE/Technology '92, (1992).
- <sup>8</sup> I.H. Malitson, JOSA vol. 55, no. 10, (1965).
- <sup>9</sup> B. Brixner, JOSA vol. 57, no. 5, (1967).
- <sup>10</sup> Technology Modeling Associates, Inc., DEPICT-2 Version 9199 (1992).

## ACKNOWLEDGEMENTS

This work is supported by the W.M. Keck Foundation and SEMATECH.

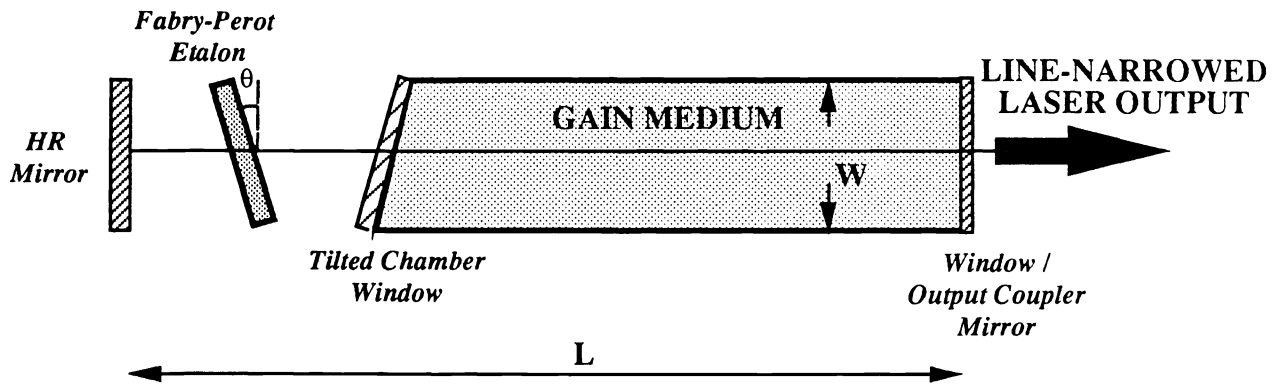


Figure 1. Excimer laser line-narrowing with intracavity etalons.

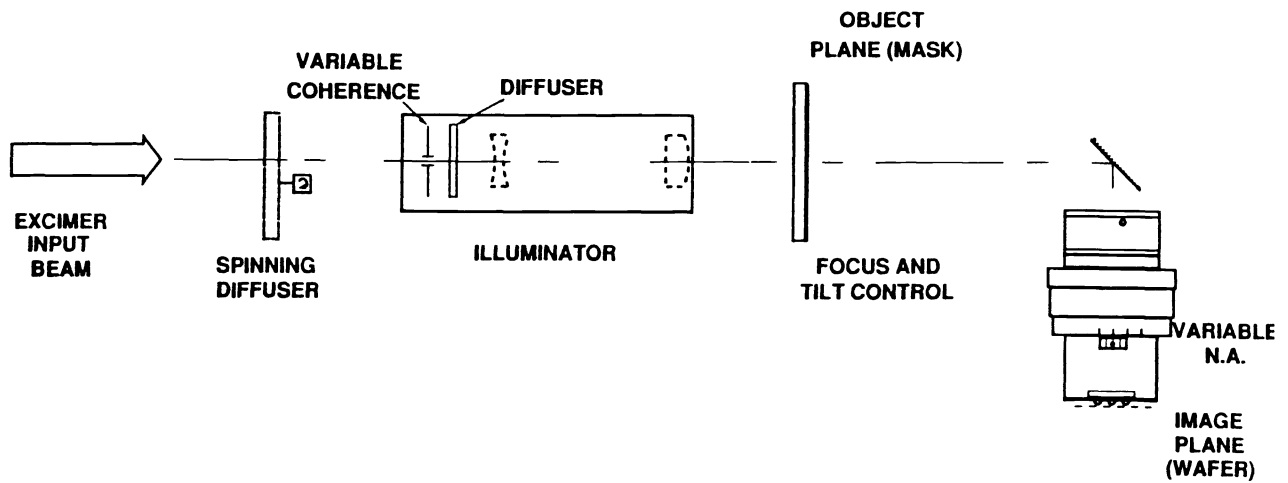


Figure 3. 20:1 ArF projection imaging system.

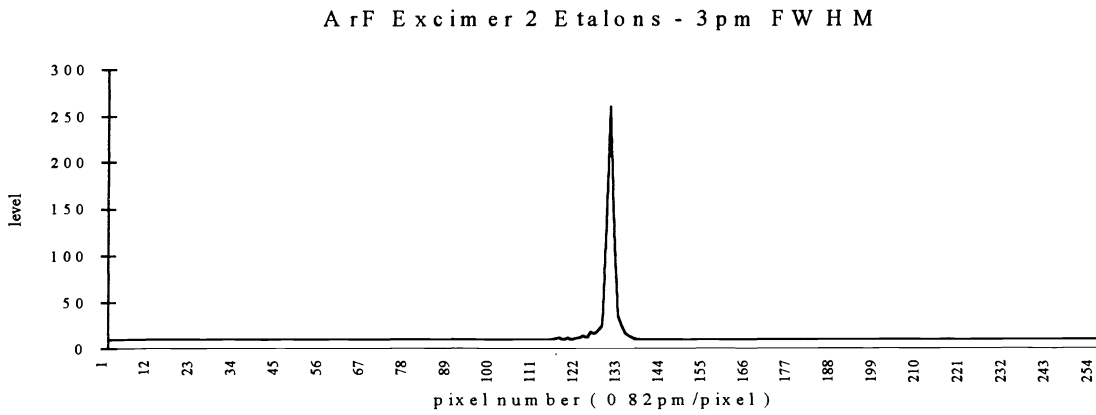
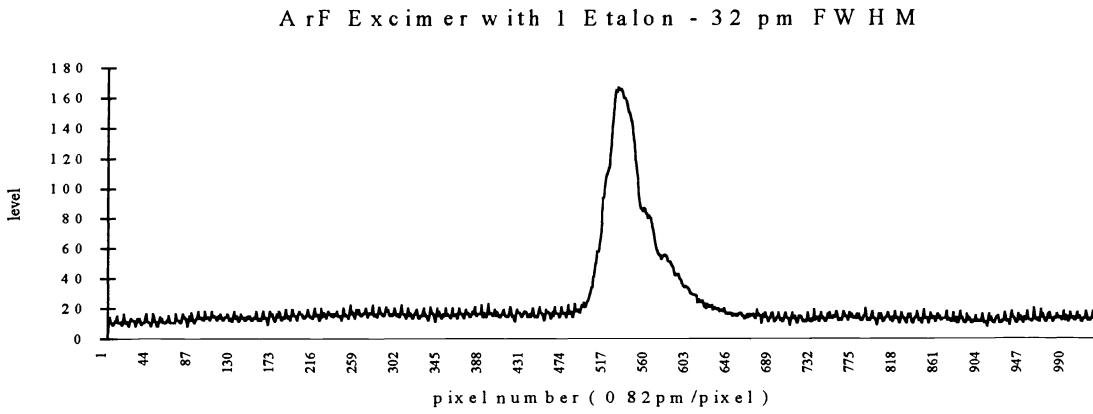
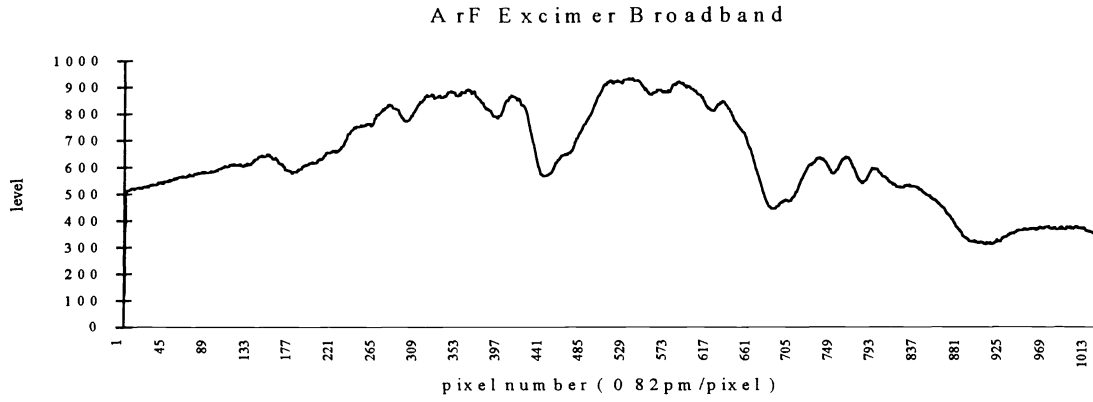


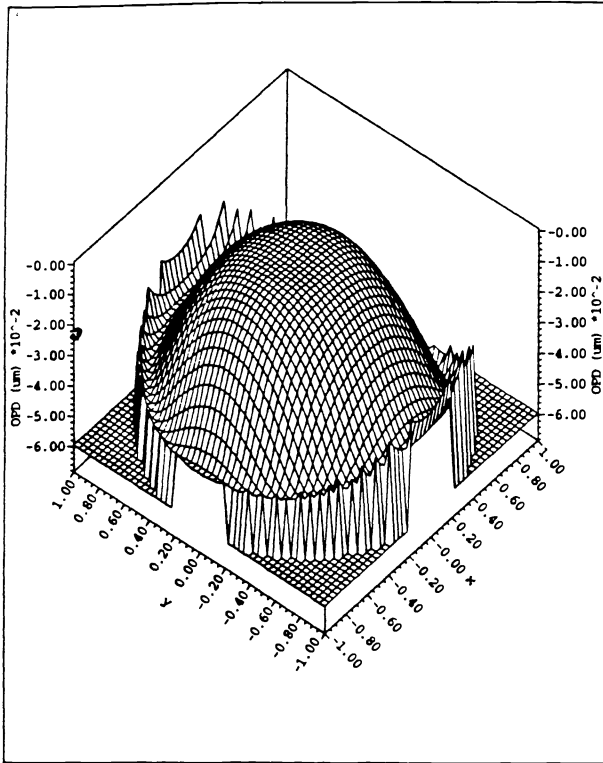
Figure 2. ArF emission - broadband, with one etalon, and with two etalons.

Term	Zernike terms at 193.300 nm			Zernike terms at 193.302 nm			Aberration
	Axis	0.7 Zone	Edge	Axis	0.7 Zone	Edge	
1	0.017	0.0131	0.0098	-0.019	-0.0234	-0.0269	Piston
2	-2E-18	-2E-18	3E-17	-1E-18	-3E-17	-3E-17	X Tilt
3	-7E-12	-0.0681	-0.1493	5E-12	-0.0756	-0.1601	Y Tilt
4	0.0133	-0.0002	-0.0151	-0.0246	-0.0386	-0.0538	Power
5	-8E-10	0.0369	0.0716	1E-09	0.0369	0.0717	3rd order astigmatism
6	-2E-19	1E-17	2E-17	2E-19	-3E-17	-4E-17	3rd order 45 astigmatism
7	9E-19	1E-17	2E-17	-5E-18	4E-18	2E-17	3rd order X coma
8	5E-13	0.0181	-0.0062	8E-12	0.0187	-0.0054	3rd order Y coma
9	0.0211	0.01	-0.0037	0.0191	0.008	-0.0058	3rd order spherical
10	-1E-19	-2E-17	-4E-17	-1E-18	-2E-17	-8E-17	
11	5E-12	0.0261	0.0771	-5E-12	0.0261	0.0771	
12	-1E-09	0.0273	0.0563	1E-09	0.0273	0.0563	5th order astigmatism
13	-2E-19	7E-18	1E-17	-5E-20	-2E-17	2E-17	5th order 45 astigmatism
14	-6E-18	-2E-17	3E-17	4E-18	-2E-17	4E-17	5th order X coma
15	2E-12	0.0212	0.0292	-1E-11	0.0212	0.0293	5th order Y coma
16	0.0294	0.0303	0.0297	0.0292	0.0302	0.0296	5th order spherical
17	-4E-06	-4E-05	-0.0002	-4E-06	-4E-05	-0.0002	
18	-5E-19	1E-17	2E-17	2E-19	-2E-17	2E-17	
19	-3E-18	-3E-17	-4E-18	-3E-18	-2E-17	-4E-17	
20	-8E-13	0.0002	0.0008	1E-11	0.0002	0.0007	
21	-1E-09	0.0041	0.0086	1E-10	0.0041	0.0085	7th order astigmatism
22	2E-19	-5E-18	-1E-17	6E-20	3E-18	2E-17	7th order 45 astigmatism
23	-4E-18	-1E-17	8E-18	9E-19	2E-17	2E-17	7th order X coma
24	1E-11	-0.0052	-0.0061	-4E-12	-0.0052	-0.006	7th order Y coma
25	0.0105	0.0125	0.0134	0.0105	0.0125	0.0134	7th order spherical
26	2E-18	-4E-18	4E-17	2E-18	3E-18	1E-17	
27	2E-12	2E-05	4E-05	3E-11	2E-05	3E-05	
28	-5E-06	-5E-06	-7E-05	-5E-06	-5E-06	-7E-05	
29	4E-20	2E-18	4E-17	-6E-19	1E-17	-3E-18	
30	-2E-18	-3E-18	-7E-18	2E-19	2E-19	8E-19	
31	-3E-12	-0.0004	-0.0009	8E-12	-0.0004	-0.0009	
32	1E-10	-0.0007	-0.0008	-1E-09	-0.0007	-0.0008	9th order astigmatism
33	-1E-19	2E-18	7E-19	2E-19	1E-17	-4E-18	9th order 45 astigmatism
34	-2E-18	-2E-17	-2E-17	-6E-18	-4E-18	6E-19	9th order X coma
35	-7E-13	0.0031	0.0035	-3E-11	0.0031	0.0035	9th order Y coma
36	0.0056	0.0051	0.0043	0.0056	0.0051	0.0043	9th order spherical
37	-0.0004	-0.0006	-0.0009	-0.0004	-0.0006	-0.0009	11th order spherical

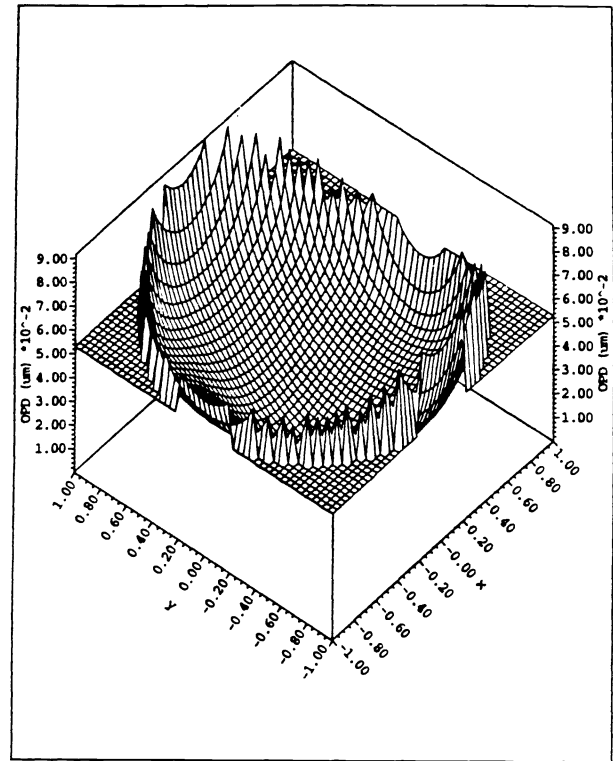
Table 1. Zernike Polynomial terms for axis, 0.70 zone, and edge field positions at 193.300 nm and 193.302 nm, in waves



OPD, defocus = -0.3  $\mu\text{m}$ , 0.70 field



OPD, defocus = 0.3  $\mu\text{m}$ , 0.70 field



OPD, defocus = 0  $\mu\text{m}$ , 0.70 field

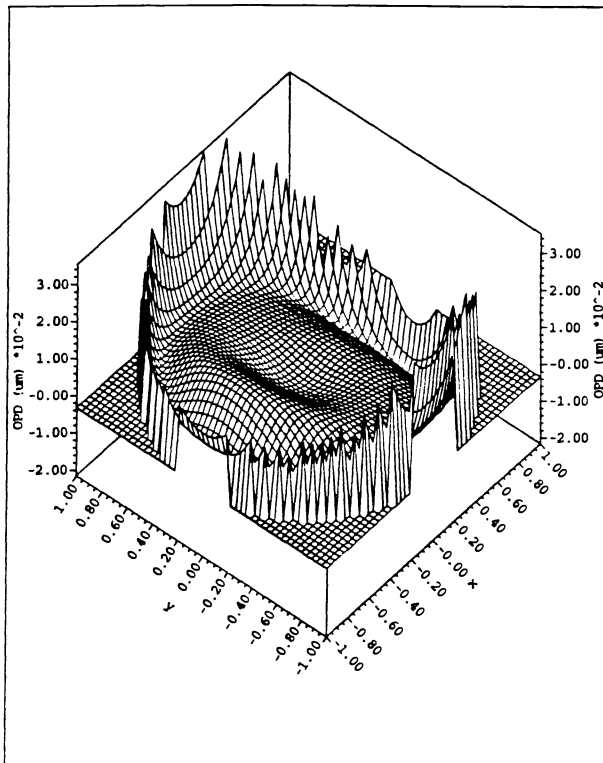
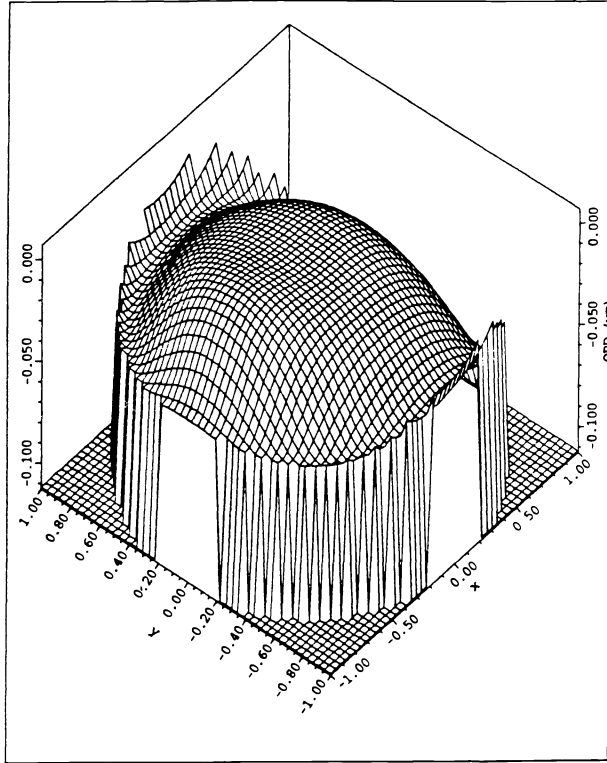
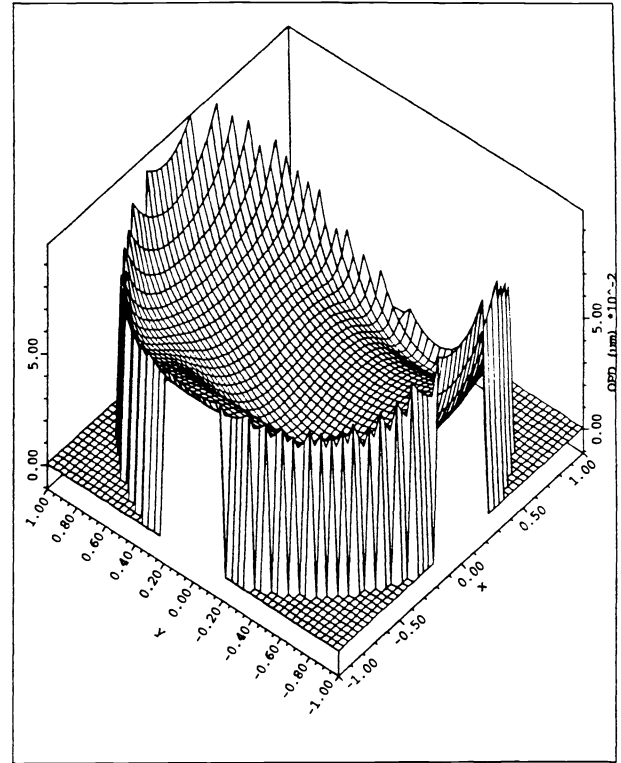


Figure 4a, b, c: Wavefront aberration plots at 0.70 field for defocus of -0.3, 0.0, and +0.3 microns.

OPD, defocus = -0.3  $\mu\text{m}$ , Full field



OPD, defocus = 0.3  $\mu\text{m}$ , Full field



OPD, defocus = 0  $\mu\text{m}$ , Full field

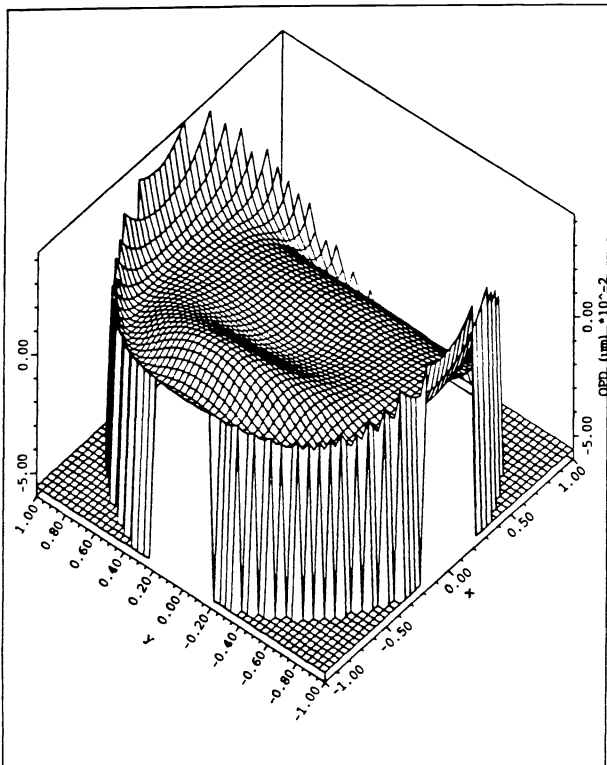


Figure 4d, e, f. Wavefront aberration plots at full field for defocus of -0.3, 0.0, and +0.3 microns.

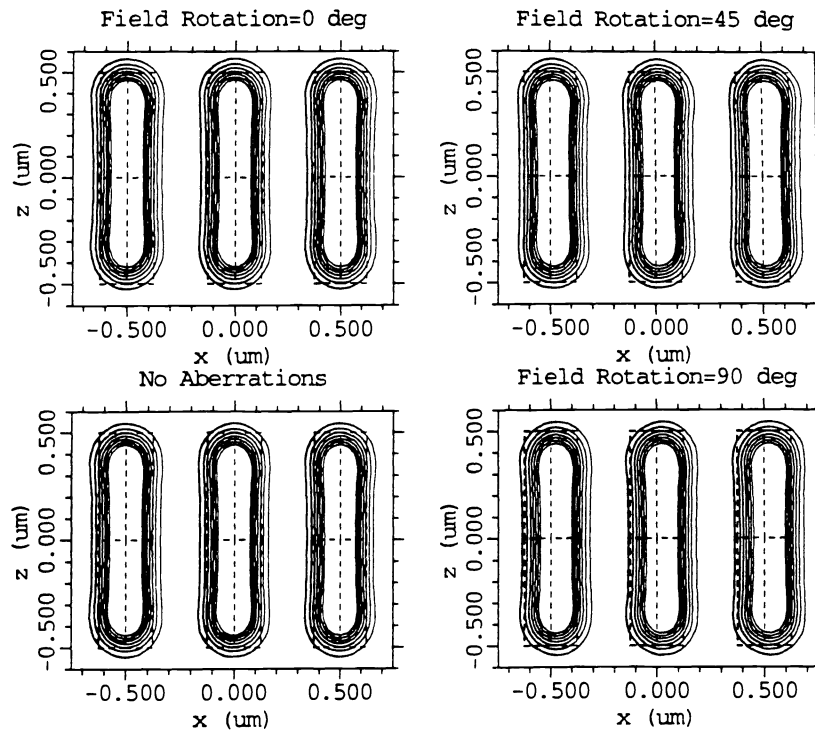


Figure 5a. Two-dimensional aerial image intensity distribution for 0.25 micron features; 0.60 NA,  $\sigma = 0.50$ , 0.70 field position.

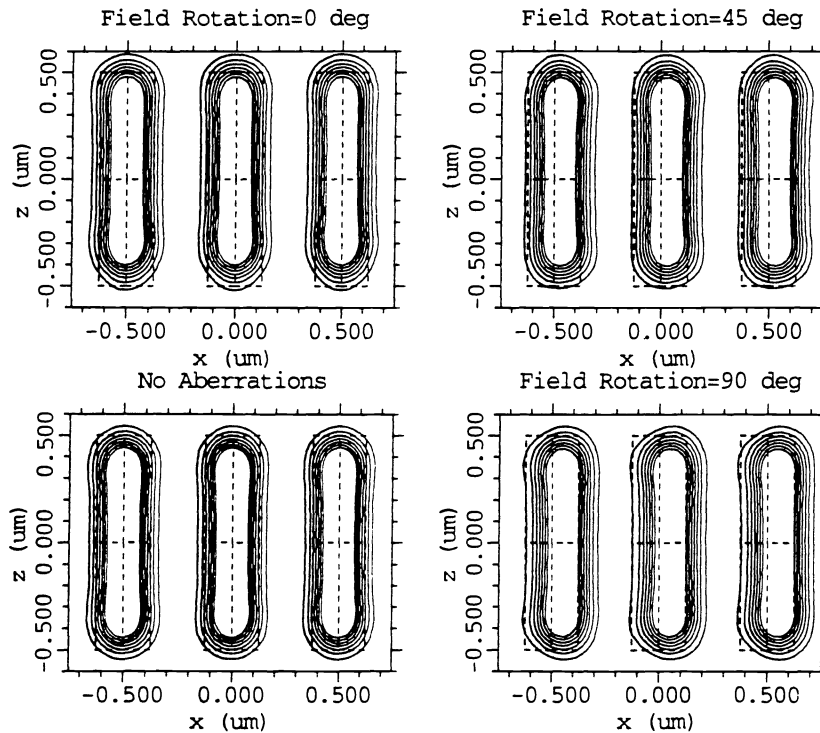


Figure 5b. Two-dimensional aerial image intensity distribution for 0.25 micron features; 0.60 NA,  $\sigma = 0.50$ , full field position.

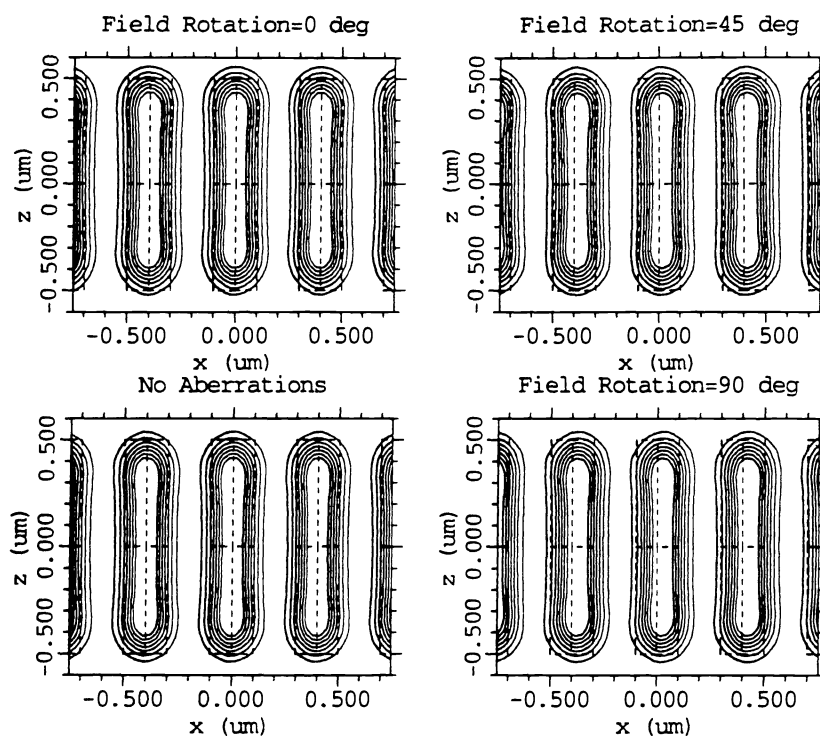


Figure 5c. Two-dimensional aerial image intensity distribution for 0.20 micron features; 0.60 NA,  $\sigma = 0.50$ , 0.70 field position.

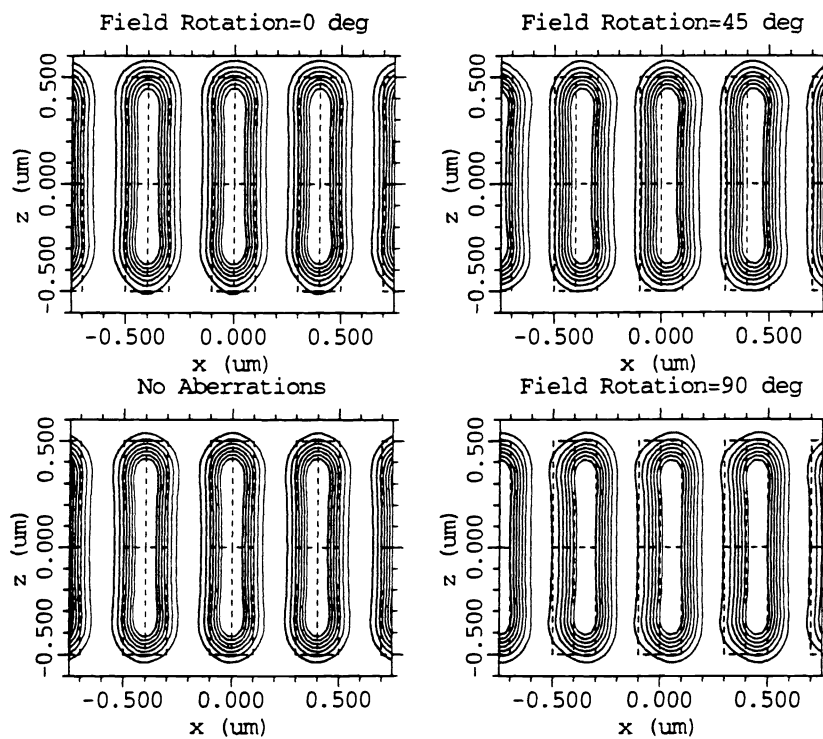


Figure 5d. Two-dimensional aerial image intensity distribution for 0.20 micron features; 0.60 NA,  $\sigma = 0.50$ , full field position.

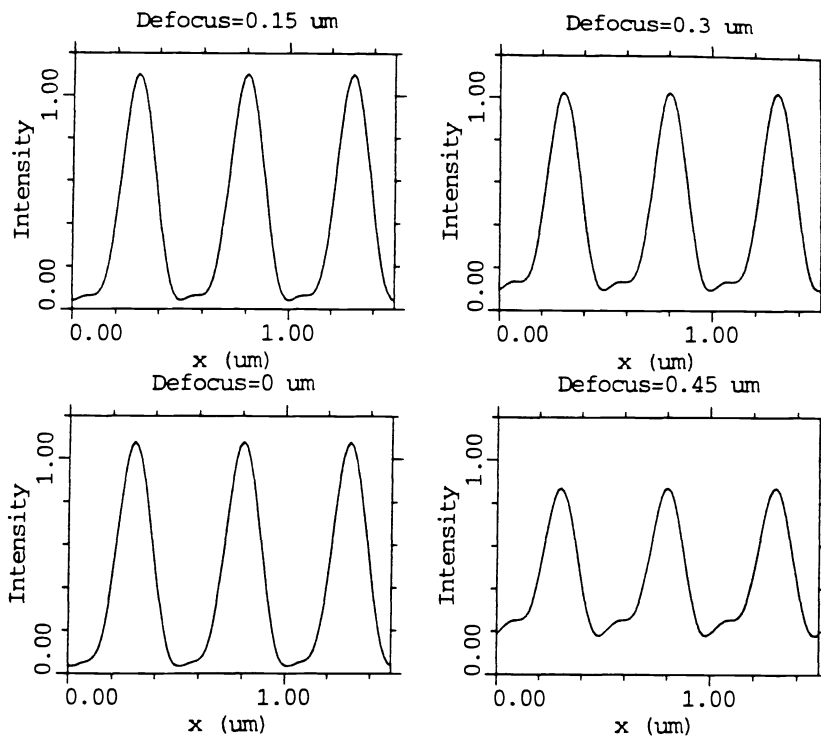


Figure 6a. One-dimensional aerial image intensity plot for 0.25 micron features; 0.60 NA,  $\sigma = 0.50$ , full field position, 0.0, 0.15, 0.3, and 0.45 micron defocus. Image modulation is 95%, 94%, 89%, and 59% for 0, 0.15, 0.30, and 0.45 micron defocus.

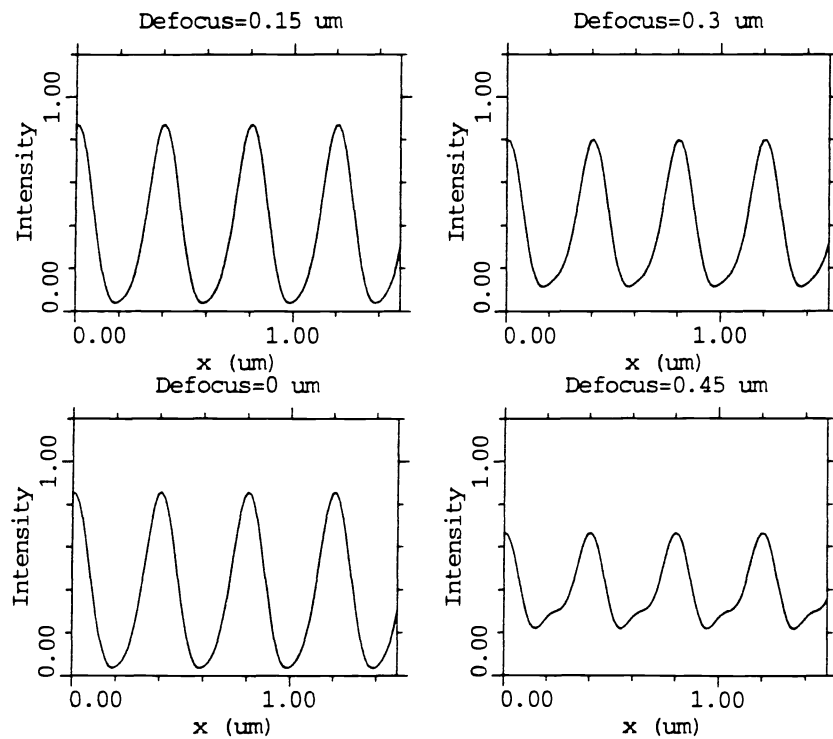


Figure 6b. One-dimensional aerial image intensity plot for 0.20 micron features; 0.60 NA,  $\sigma = 0.50$ , full field position, 0.0, 0.15, 0.3, and 0.45 micron defocus. Image modulation is 91%, 89%, 73%, and 40 % for 0, 0.15, 0.30, and 0.45 micron defocus.